Comparisons between WAVE and seismological data

by A. Daehnke*

Synopsis

In order to test the applicability of elastodynamic codes in the modelling of mining-related problems, comparisons are made between seismic data and numerical analyses. The dynamic finite-difference program WAVE is used for the modelling of a horizontal stope in a deep mine. The slip along a vertical fault situated within the positive excess shear stress lobe of the stope initiates seismic waves. The stope-fault geometry is modelled in both two and three dimensions.

The three-dimensional non-slip-weakening WAVE analyses correlate well with Brune's analytical model. For accurate modelling of the peak particle velocities predicted by McGarr's empirical relationship, it is recommended that a three-dimensional stope-fault model is used, with the amount of slip weakening dependent on the magnitude of the event.

* *Mining Technology Rock Engineering, P.O. Box 91230, Auckland Park, 2006 Gauteng.*

 SA ISSN 0038-223X/3.00 + 0.00. Paper received Sep. 1994; revised paper received Mar. 1995.

Introduction

This paper sets out the results of an investigation into the correlation of numerically predicted elastodynamic ground movements and seismological field data so that the suitability of these programs for the modelling of mining-related problems can be assessed. The elastodynamic finite-difference program WAVE is used in a comparison of fault slip and the resulting wave propagation with seismological data. Peak particle velocities calculated by WAVE are correlated with analytical models and seismic field studies.

The objectives of this investigation were as follows:

- to model fault slip and wave propagation in two and three dimensions
- to determine the effect of a reduction in fault cohesion according to a slip-weakening law
- to compare the far-field attenuation of peak particle velocity as calculated by WAVE with that of the analytical model of Brune[1,2] and the empirical relationship of McGarr[3]
- to correlate the near-field peak particle velocities and velocity amplification factors calculated by WAVE with seismological studies conducted by Spottiswoode and Churcher[4].

The paper begins by describing the numerical two- and three-dimensional WAVE model used in the investigation. The far-field peak particle velocities and near-field amplification factors and peak velocities are then correlated. Finally, conclusions are drawn as to the effectiveness of WAVE in the modelling of dynamic mining-related problems, and recommendations are made.

The WAVE model

A horizontal stope of 60 m span is subjected to a stress field at a depth of 2600 m below surface of 70 MPa in the vertical and 35 MPa in the horizontal direction. The stress field interacts with the stope and generates the zero excess shear stress (ESS) contour (Napier[5], Ryder[6]) depicted in Figure 1. The ESS can be defined as the difference between the prevailing shear stress prior to slip and the dynamic strength of the fault plane. Thus,

$$ESS = |\tau| - \mu\sigma_n,$$

where $\mu = \tan\phi$ and ϕ is the friction angle, τ is the shear stress, and σ_n is the normal stress. In this study, the friction angle on the fault interface is assumed to be 10 degrees. A vertical fault is situated ahead of the stope and, with no cohesion on the fault interface, the section of the fault contained within the zero ESS contour will rupture.

WAVE is a finite-difference code that is able to model wave propagation in a two- or three-dimensional elastic medium. Second-order interlaced finite-difference equations are used on an orthogonal grid with uniform grid spacing. WAVE has the ability to model dislocations that can represent faults or tabular stopes.

The WAVE analyses are completed in two steps.

- In Step 1, the fault is locked by the application of a high cohesion to the interface, the external stress field is applied, and WAVE is cycled until the stope reaches an equilibrium closure when the maximum velocities in the finite-difference mesh are negligible.

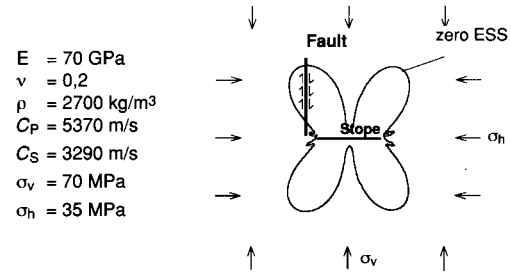

Figure 1—The two-dimensional WAVE model, where E is Young's modulus, ν is Poisson's ratio, ρ is rock density, and C_P and C_S are respectively the P- and S-wave velocity

Comparisons between WAVE and seismological data

Thus, WAVE can be calibrated, by adjustment of the amount of slip weakening, to match far-field seismological data.

In the near-field, WAVE is used in the calculation of hangingwall velocity amplification factors and peak velocities. The amplification factors compare well with those measured in a field study conducted by Spottiswoode and Churcher. A method is proposed for the identification of potentially hazardous stope areas prone to excessive velocities.

- In Step 2, the fault cohesion is reduced and the fault ruptures. Fault cohesion is either set to zero instantaneously, resulting in sudden fault rupture along the length of the fault situated within the zero ESS lobe, or a slip-weakening law is applied to the fault interface. In the latter case, the cohesion along the whole fault is reduced so that slip just commences at a point on the fault. As slip occurs at this point, the cohesion is reduced linearly (Figure 2), and the shear stress is increasingly transferred to adjacent grid points until they slip. Thus, by the application of a slip-weakening law to the fault interface, fault slip occurs progressively. A progressive fault-rupture model is considered to be more realistic than an instantaneous fault-rupture model.

The sequence of snapshots in Figures 3, 4, and 5 illustrate the absolute velocity in the two-dimensional geometry outlined in Figure 1 at 11, 24, and 30 ms after sudden fault rupture, i.e. the fault cohesion is zeroed instantaneously. The fault and stope are oriented parallel to the y- and x-axes respectively.

The waves displayed in the carpet plots of Figures 3 to 5 can be categorized according to the following types.

- A strong shear wave demarcated by **S** propagates away from the fault.
- A Rayleigh wave (**R**) propagates along the stope hangingwall.
- The faster P-wave (**P**) has propagated further than the shear or Rayleigh waves, but absolute velocities within the P-wave are small compared with the peak velocities associated with the shear or Rayleigh waves.

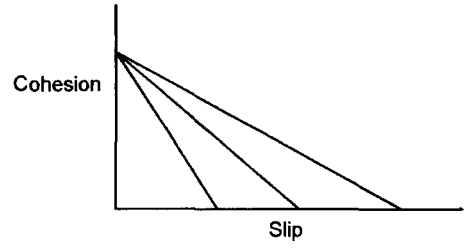

Figure 2—The WAVE slip-weakening relationship for three slip-weakening rates

In Figure 4, the Rayleigh wave has propagated along the length of the stope hangingwall and, since its propagation speed is 2980 m/s versus 3290 m/s for the speed of the shear wave, it lags behind the front of the shear wave. The P-wave is about to propagate beyond the window for which the carpet plot was created. After 30 ms (Figure 5), the Rayleigh wave is reflected at the stope end and then propagates along the footwall back towards the fault.

The P- and S-waves emitted by a progressively rupturing fault are not as clearly defined as the waves radiating from a suddenly rupturing fault. During progressive rupture, multiple P- and S-waves are initiated, and the overall wave pattern is noisy and complicated. However, the Rayleigh waves propagating along the stope surfaces are equally prominent in the analyses of sudden and progressive fault rupture.

The three-dimensional WAVE model comprises a vertical fault situated ahead of a horizontal 60 x 60 m stope. The fault-slip model is identical to the two-dimensional case: both the sudden fault rupture and the progressive slip-weakening case are investigated. The three-dimensional model is discretized into a grid of 82 x 64 x 64 elements consisting of 3 x 3 x 3 m elements. Figure 6 depicts three views of the three-dimensional ESS lobe in the plane of the fault. The section of the fault intersecting the ESS lobe will rupture.

Figure 7 shows the evolution of absolute slip on the planar fault at $t = 3$ and 10 ms, and the final slip profile at $t = 20$ ms for a slip-weakening model that linearly reduces cohesion to zero after a relative slip of 0,1 mm.

Correlation of far-field peak particle velocities

In this section, the attenuation of far-field peak particle velocity calculated by WAVE is compared with the analytical model of Brune[1,2] and an empirical relationship determined by McGarr[3].

The Brune model

Brune[1,2] presented a model of the seismic source in which the fault is represented as a circular area. A shear-stress loading is applied to a circular area on the fault surfaces at time zero, resulting in the propagation of a pure wave of shear stress perpendicular to the dislocation surface. The effects of fault propagation and friction are neglected in the Brune[1,2] model. Thus, Brune's model can be closely compared with the WAVE analyses where fault cohesion is eliminated instantaneously. He determined the initial near-field peak particle velocity to be

$$\dot{u} = \frac{\Delta\tau}{G}\beta,$$

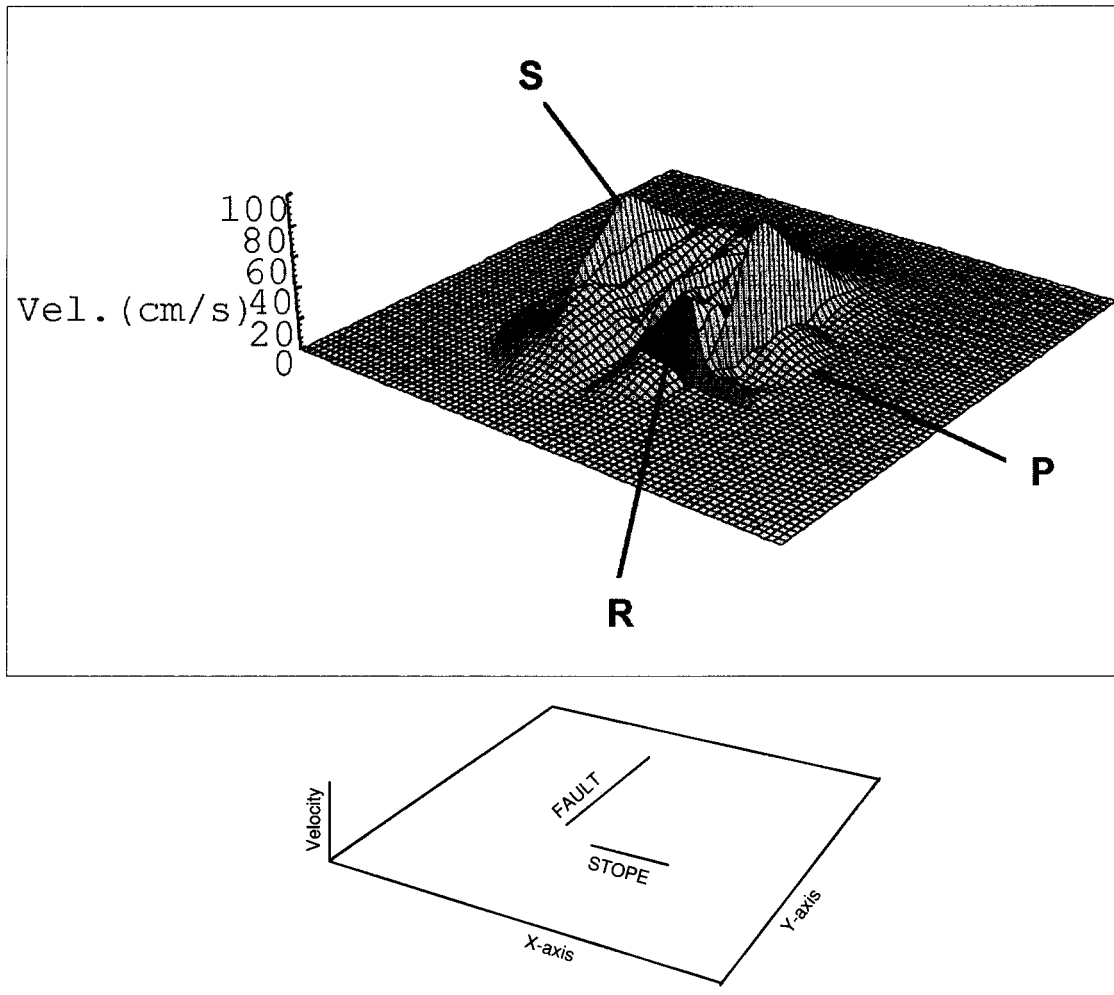

Figure 3—Carpet plot of the absolute velocity at t = 11 ms. Also shown is a schematic diagram indicating the fault and stope positions

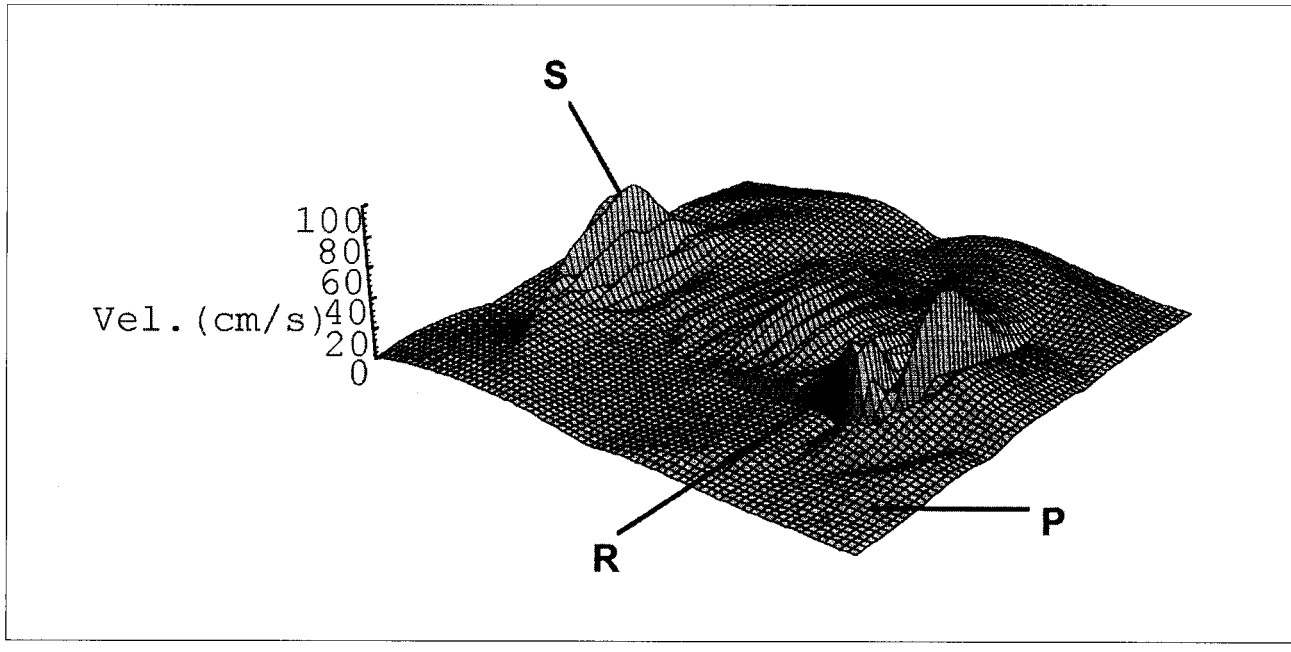

Figure 4—Absolute velocity at t = 24 ms

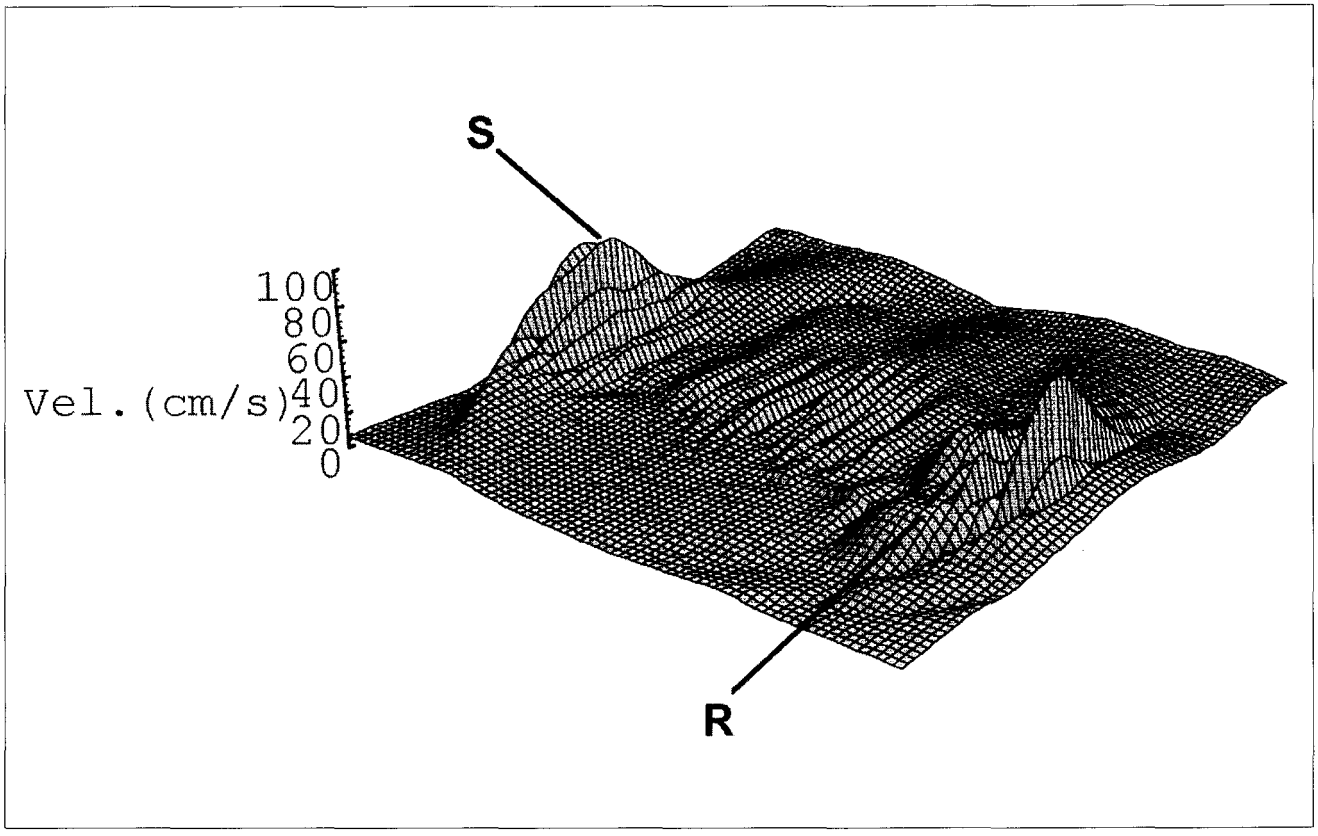

Figure 5—Absolute velocity at t = 30 ms

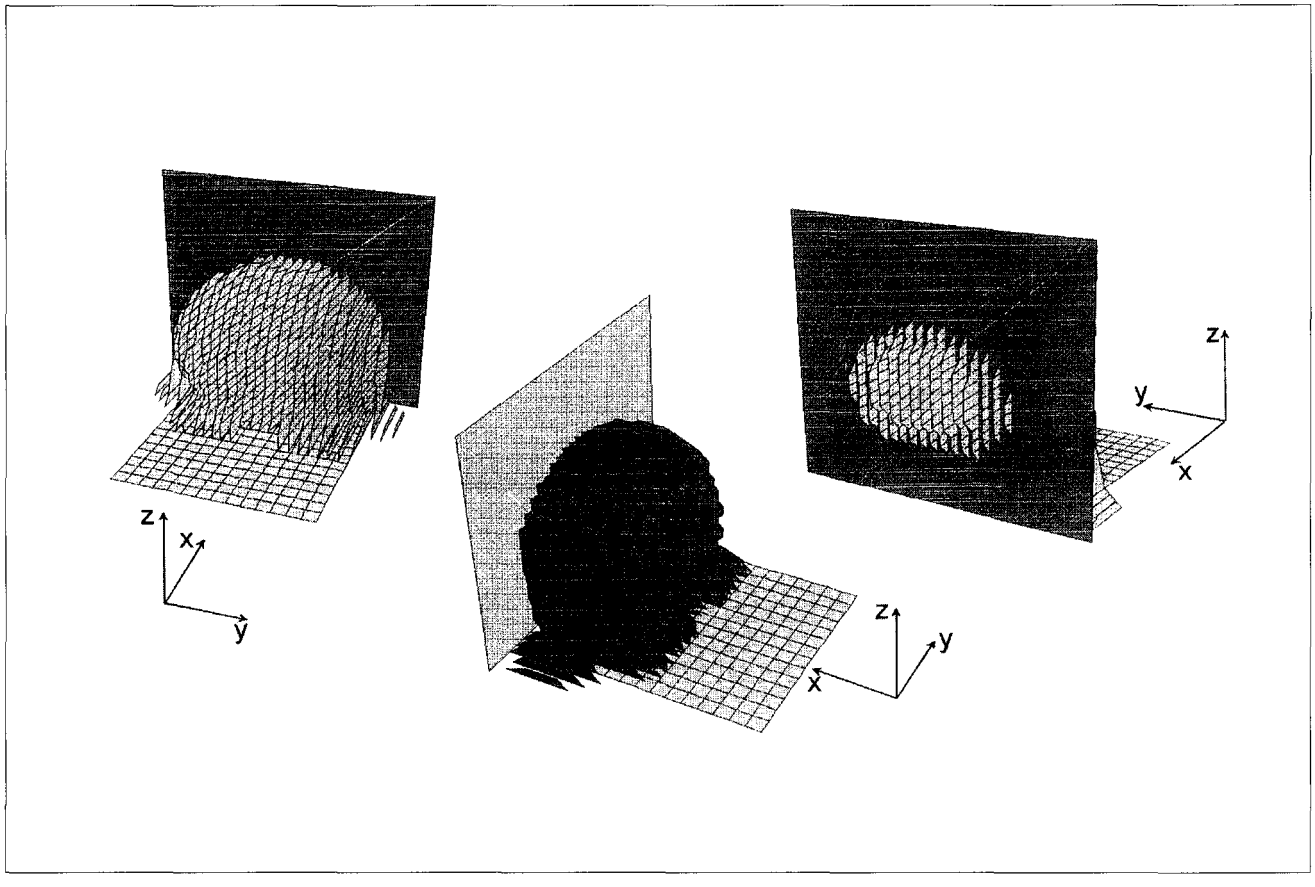

Figure 6—The three-dimensional ESS lobe intersecting the fault

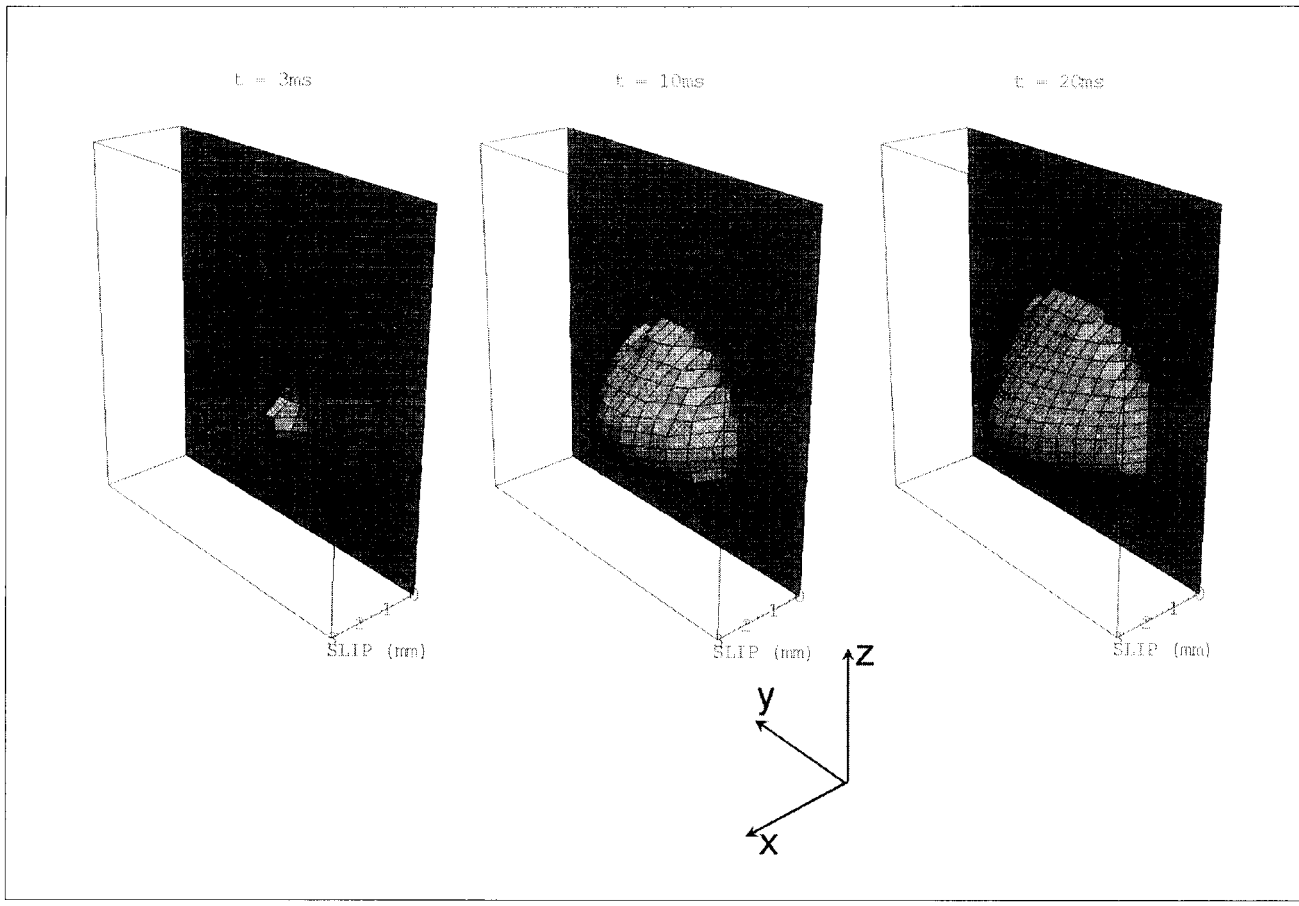

Figure 7—Evolution of absolute slip on a planar fault where the slip-weakening model reduces fault cohesion to zero after a slip of 0,1 mm

where $\Delta\tau$ is the shear-stress pulse, G is the bulk modulus, and β is the shear wave velocity. The displacement of far-field peak particle is given by

$$u(t) = R_{\theta\phi}\frac{\Delta\tau\beta r_o}{GR}te^{-\omega_o t}, \qquad [1]$$

where $R_{\theta\phi} = 0,57$ is the median value of the radiation factor for a double-couple source calculated at 1000 points randomly distributed over the focal sphere (Spottiswoode and McGarr[7]), $\omega_0 = 2\pi f_0$, R is the hypocentral distance, r_0 is the source radius, and t is the retarded time related to the time after the event t' by $t = t' - R/\beta$; for $t < 0$, $u(t) = 0$. Differentiating equation [1] with respect to time yields

$$\dot{u}(t) = R_{\theta\phi}\frac{\Delta\tau\beta r_o}{GR}e^{-\omega_o t}(1-\omega_o t),$$

and, noting that the peak velocity occurs at the retarded time $t = 0$,

$$RV_{max} = 0,57\frac{\Delta\tau\beta r_o}{G}.$$

From Brune[1,2], $\Delta\tau = \frac{7}{16}\frac{M_o}{r_o^3}$,

thus

$$RV_{max} = 0,57\frac{\Delta\tau\beta}{G}\sqrt[3]{\frac{7M_o}{16\Delta\tau}}. \qquad [2]$$

Equation [2] is used in the calculation of the analytical velocity attenuation as predicted by Brune's model[1,2]. The shear stress difference, $\Delta\tau$, before and after fault rupture is determined for each stope–fault geometry by calculation of the average ESS on the fault plane that intersects the positive ESS lobe. The fault position is varied in 3 m increments (the element size) from 6 to 27 m ahead of the stope. For the two-dimensional geometries, the drop in shear stress was found to vary from 5,3 MPa for a fault situated 9 m ahead of the stope to 0,4 MPa for a fault 27 m from the stope. In three dimensions, the stress drop ranged from 4 MPa for a fault 6 m ahead of the stope to 0,2 MPa for a fault 15 m ahead. The stress drops were found to be compatible with mine seismic data (McGarr[3], Spottiswoode[8]).

References

1. BRUNE, J. N. Tectonic stress and the spectra of seismic shear waves from earthquakes. *J. Geophys. Res.*, vol. 75. 1970. pp. 4997-5009.
2. BRUNE, J. N. Tectonic stress and the spectra of seismic shear waves from earthquakes (correction). *J. Geophys. Res.*, vol. 76. 1971. p. 5002.
3. MCGARR, A. Scaling of ground motion parameters, state of stress and focal depth. *J. Geophys. Res.*, vol. 89. 1984. pp. 6969-6979.

Empirical relationships relating RV_{max} to seismic moment

Brune's model[1,2] and peak particle velocities calculated by WAVE are compared with an empirical relationship that relates the product of hypocentral distance and peak particle velocity to seismic moment. The majority of published papers relating such relationships have concentrated on seismic events of large magnitude, the measurements made being at large distances from the seismic source. McGarr *et al.*[9] provided the first relationship for mine tremors based on 12 events. Other studies relating the attenuation of peak particle velocity in mine tremors to the size of the event have been conducted by, amongst others, Spottiswoode[10], McGarr[3], Hedley[11], and Butler and Van Aswegen[12]. In the present investigation, the following relationship by McGarr[3], based on 24 mining-induced events and 28 non-mining related events, is used:

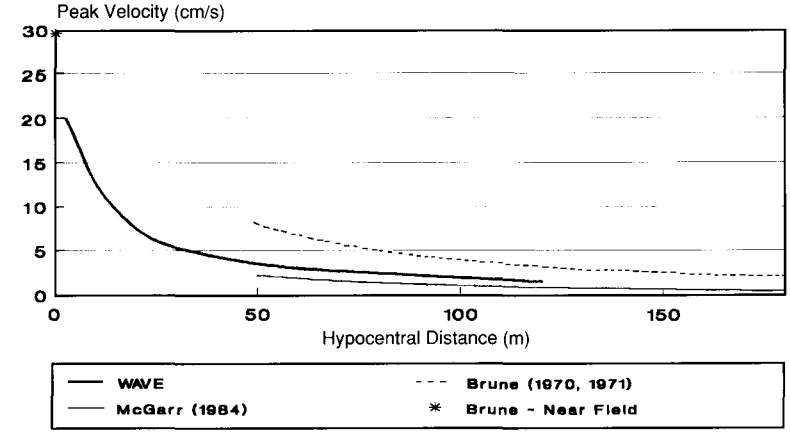

Figure 8—Three-dimensional velocity attenuation as predicted by WAVE, the analytical model of Brune[1,2], and the empirical relationship of McGarr[3] (fault 9 m ahead of stope, M_o = 98 GNm, M_L = 1,6, and r_o = 25 m)

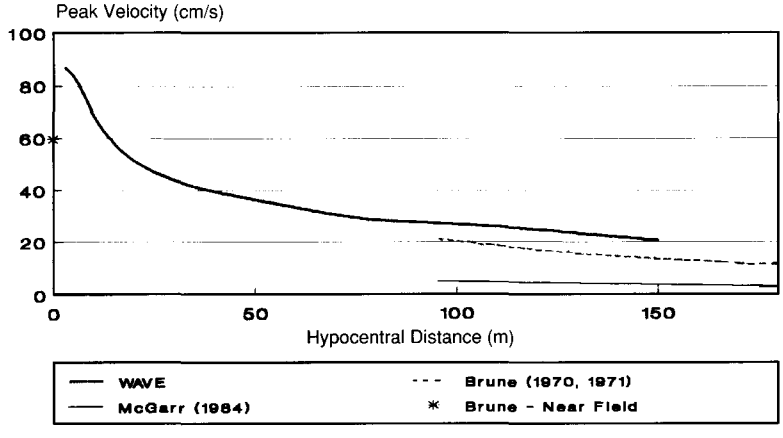

Figure 9—Two-dimensional velocity attenuation (fault 9 m ahead of stope, M_o = 2500 GNm, M_L = 2,7, and r_o = 48 m)

$$\log (RV_{max}) = -4{,}78 + 0{,}44 \log (M_o),$$

where R is the hypocentral distance in m, V_{max} is the peak particle velocity in m/s, and M_o is the seismic moment in Nm.

Peak particle velocity

To relate the far-field peak particle velocities of the numerical analysis to analytical and seismological data, the peak velocities are calculated by WAVE along a line extending perpendicular to the fault away from the stope. The line, which is drawn from the point of maximum fault slip, represents the location at which, for any given time instant, the peak particle velocities occur in the numerical model. Figure 8 depicts the variation of hypocentral distance versus peak velocity for the three-dimensional model with a fault situated 9 m ahead of the stope. With $M_o = GDA$ (Aki and Richards[13]), where M_o is the seismic moment, G is the bulk modulus, D is the average absolute slip over the rupture area, and A represents the rupture area, the seismic moment for this stope-fault geometry is calculated to be 98 GNm. The local magnitude on the Richter scale can be related to the seismic moment on an empirical basis. A number of such empirical relations have been derived from actual data. They are all expressed in the same form, but with slightly different parameter values. Thus, the average of $\log M_o = 8{,}7 + 1{,}2M_L$ (Spottiswoode and McGarr[7]), $\log M_o = 10{,}2 + 1{,}2M_L$ (Gibowicz[14]), $\log M_o = 9{,}2 + 1{,}3M_L$ (Brummer and Rorke[15]), and $\log M_o = 7{,}05 + 1{,}5M_L$ (Hanks and Kanamori[16]) is used to estimate the event magnitude as $M_L \approx 1{,}6$. The average source radius for this event is 25 m. In this study, the far field is assumed to be greater than twice the source radius[17]. Also shown in Figure 8 are the far- and near-field peak particle velocities predicted by the analytical model of Brune[1,2] and the attenuation of far-field peak velocity predicted by the empirical relationship of McGarr[3].

The WAVE velocity attenuation depicted in Figure 8 is radiating from a progressively rupturing fault, i.e. a slip-weakening law is applied to the fault interface, where fault cohesion is linearly reduced to zero after a relative slip of 0,1 mm. Thus it is expected that the sudden fault-rupture model of Brune[1,2] will predict higher velocities than WAVE. The empirical relationship of McGarr[3] predicts lower peak velocities than the WAVE and Brune models.

The velocity attenuation in Figure 8 is shown for the two-dimensional case in Figure 9. The fault is again 9 m ahead of the stope and, on the assumption of a circular rupture plane as suggested by Sjöberg[18] in his two-dimensional analyses, the seismic moment is 2500 GNm and the source radius is 48 m. Compared with the three-dimensional case, the plane strain assumption in the two-dimensional WAVE model generates a more extensive zero ESS zone, rupture occurs along a greater fault length, and a larger event is generated.

4. SPOTTISWOODE, S. M., and CHURCHER, J. M. The effect of backfill on the transmission of seismic energy. *Backfill in South African mines.* Johannesburg, South African Institute of Mining and Metallurgy, 1988. pp. 203–217.

In an evaluation of the effect of slip weakening and an increasing distance from the fault to the stope, the attenuation of peak particle velocity was calculated for numerous two- and three-dimensional WAVE models.

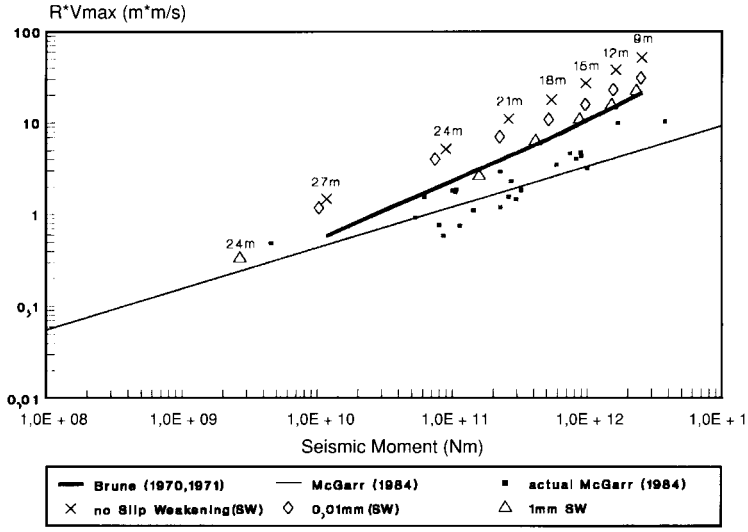

Figure 10—Velocity attenuation as calculated by the two-dimensional WAVE model. The markers (crosses, diamonds, triangles) are labelled with the stope-to-fault distance for each model geometry analysed. In the case of the markers representing one model geometry (but various degrees of slip weakening) lying directly below one another, only one label is used to specify the stope-to-fault distance. Also shown are the results of the analytical Brune[1,2] model and the empirical relationship of McGarr[3]

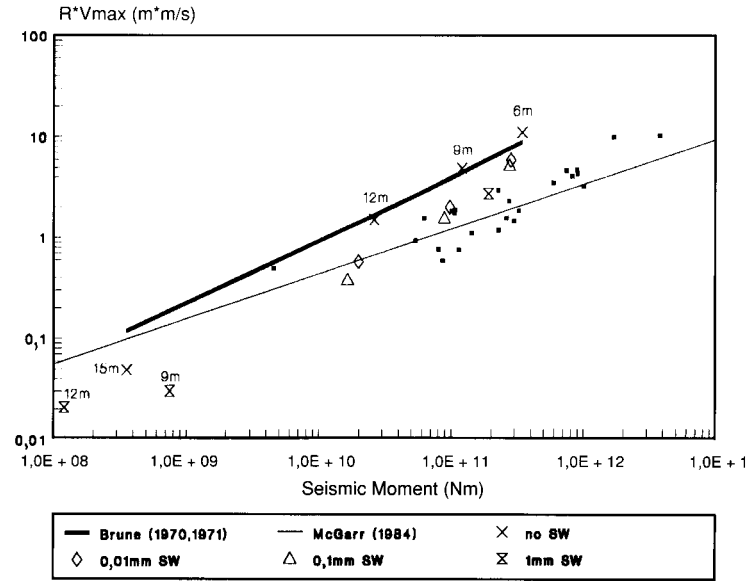

Figure 11—Velocity attenuation as calculated by the three-dimensional WAVE model. Also shown are the results by the analytical model of Brune[1,2] and the empirical relationship of McGarr[3]

The far-field peak particle velocity calculated by WAVE was found to be approximately inversely proportional to the hypocentral distance, i.e. $RV_{max} \approx$ constant. The average standard deviation of the hyperbola fit (RV_{max} = constant) for the 13 three-dimensional models was 4,9 per cent whilst, for the 20 two-dimensional models, the average standard deviation was 7,2 per cent. When the attenuation of far-field peak particle velocity was represented by an RV_{max} product, a single log–log chart, the abscissa representing seismic moment and the ordinate depicting the RV_{max} product, could be plotted for the comparison of numerical analyses with various degrees of slip-weakening and a range of stope-to-fault distances.

Figure 10 displays such a graph for the two-dimensional model for stope-to-fault distances ranging in 3 m increments (the element size) from 9 to 27 m with an instantaneously rupturing fault, and 0,01 and 1 mm slip weakening. Also shown are the analytical model of Brune[1,2] and the McGarr[3] empirical relationship. Some of the 52 actual McGarr[3] events are also plotted.

Figure 10 indicates that the magnitude of the event decreases with increasing stope-to-fault distance. It decreases slightly with an increasing degree of slip weakening, but more slip weakening strongly reduces the RV_{max} product. The two-dimensional plane-strain approximation over-estimates the far-field peak particle velocities, and the two-dimensional WAVE analyses predict higher peak particle velocities than the models of Brune[1,2] and McGarr[3].

The velocity attenuation for the three-dimensional WAVE model, the Brune[1,2] model, and McGarr's empirical[3] relation is shown in Figure 11. The WAVE models were analysed for stope-to-fault distances of 6 to 15 m, and for an instantaneously rupturing fault and slip weakening of 0,01 mm, 0,1 mm, and 1 mm. Whereas, in the two-dimensional analysis, rupture occurs along a fault situated up to 27 m ahead of the stope, the three-dimensional zero ESS lobe extends only 15 m ahead of the stope; thus, no rupture occurs if the fault is situated further than 15 m ahead of the stope.

The three-dimensional instantaneous fault-rupture WAVE model correlates well with Brune's model[1,2], which also analyses an instantaneously rupturing fault, and it is encouraging to note that the numerical analyses compare well with the analytical solution. As in the two-dimensional case, when the degree of slip-weakening is reduced, the RV_{max} product is strongly reduced.

5. NAPIER, J. A. L. The application of excess shear stress to the design of mine layouts. *J. S. Afr. Inst. Min. Metall.*, vol. 87. 1987. pp. 397–405.
6. RYDER, J. A. Excess shear stress in the assessment of geologically hazardous situations. *J. S. Afr. Inst. Min. Metall.*, vol. 88. 1988. pp. 27–39.
7. SPOTTISWOODE, S. M., and MCGARR, A. Source parameters of tremors in a deep-level gold mine. *Bull. Seism. Soc. Am.*, vol. 65. 1975. pp. 93–112.
8. SPOTTISWOODE, S. M. Seismic attenuation in deep-level mines. *Rockbursts and seismicity in mines.* Young (ed.). Rotterdam, Balkema, 1993. pp. 409-414.
9. MCGARR, A., GREEN, R.W.E., and SPOTTISWOODE, S.M. Strong ground motion of mine tremors: some implications for near-source ground motion parameters. *Bull. Seism. Soc. Am.*, vol. 71. 1981. pp. 295–319.
10. SPOTTISWOODE, S.M. Underground seismic networks and safety. *Monitoring for safety in geotechnical engineering.* Johannesburg, SANGORM, 1984.
11. HEDLEY, D.G.F. Peak particle velocity for rockbursts in some Ontario mines. *Rockbursts and seismicity in mines.* Fairhurst (ed.). Rotterdam, Balkema, 1990. pp. 345–348.

The numerical values follow a steeper trend line compared with the McGarr[3] relationship and Brune's model[1,2]. This might be due to the slip-weakening logic applied to the fault interface, and it is recommended that alternative cohesion-weakening logic, such as velocity weakening, should be investigated. By the incorporation of alternative cohesion-weakening logic, numerical models might yield superior approximations of the far-field peak particle velocities, at increasing fault-to-stope distances, than the slip-weakening model used in this study. In the interim, to closely approximate seismological far-field velocities, the appropriate degree of slip weakening needs to be chosen. Faults close to the stope need to be modelled with a high degree of slip weakening (≈ 1 mm), whereas faults further from the stope should be modelled with less slip weakening.

Comparisons of near-field velocities

Spottiswoode and Churcher[4] and Hemp and Goldbach[19] investigated near-field peak particle velocities measured by geophones placed in the footwall and hangingwall. They calculated a velocity amplification factor by comparing the footwall and hangingwall velocities with velocities predicted at the same distance from the source, but in the rock massif. The velocity amplification factor is a convenient measure of the effect of the Rayleigh wave propagating along stope surfaces. In the present study, the same approach was followed: velocities were measured along the footwall and hangingwall, and were then compared with velocities at equivalent hypocentral distances (on the opposite side of the fault) in the solid rock mass.

The velocity amplification factor is calculated for the vertical and horizontal velocity components in two and three dimensions. Figure 12 is a graph of the hangingwall velocity amplification factor versus the position in the stope, measured from the stope face. The open stope extends from 0 to 60 m. Thus, as shown in Figure 12, the amplification factor is approximately unity in the solid rock ahead of the stope (< 0 m) and behind the stope (> 60 m). Along the open stope, the Rayleigh wave amplifies hangingwall velocities by a factor of 2,5 to 3,0 in the horizontal direction and 1,5 to 2,4 in the vertical direction. Solutions of the two-dimensional model correlate well with those given by the three-dimensional model, indicating that the Rayleigh-wave effect can be modelled accurately by the two-dimensional plane-strain model. The exception is a peak in the horizontal velocity amplification factor calculated by the three-dimensional model at the stope end. No explanation can be given at this stage for the peak, and further research is necessary into the mechanism generating the high amplification at that position.

Spottiswoode and Churcher[4] measured 50 events with geophones placed in the footwall and hangingwall initially 10 m from the stope face, and later, as mining progressed, 20 m from the face. As indicated in Figure 12, the WAVE analyses compare well with their results.

Spottiswoode and Churcher[4] noted that, where they could locate the focal point of the event above the stope, the hangingwall experienced higher levels of ground motion than the footwall. Thus, the stope cast a partial shadow across the incoming rays. These findings were confirmed by the numerical analyses, and the footwall amplification factors ranged between 0,4 and 1,1.

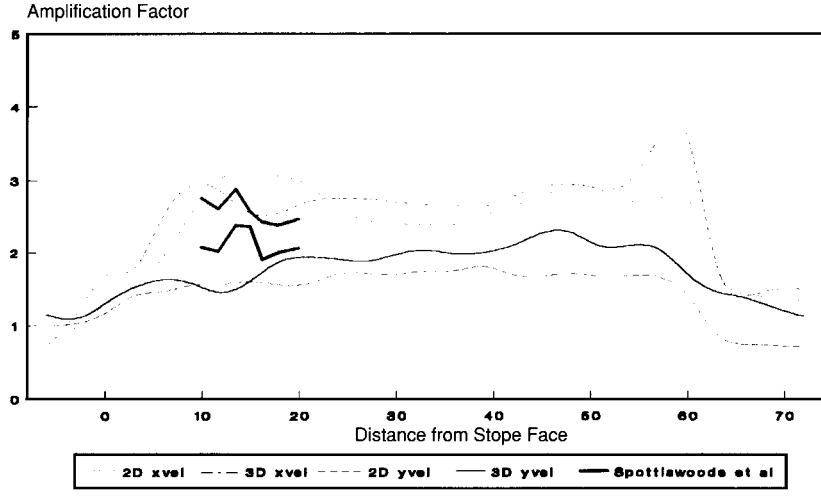

Figure 12—Hangingwall velocity amplification for an event generated by a fault 9 m ahead of the stope face (xvel and yvel refer to the horizontal and vertical velocity amplification factors respectively)

12. BUTLER, A.G., and VAN ASWEGEN, G. Ground velocity relationships based on a large sample of underground measurements in two South African mining regions. *Rockbursts and seismicity in mines.* Young (ed.). Rotterdam, Balkema, 1993. pp. 41–48.
13. AKI, K., and RICHARDS, P.G. *Quantitative seismology: theory and methods.* San Francisco, Freeman, Cooper, 1980. vol. 1, chap. 3, p. 49.
14. GIBOWICZ, S.J. Variation of source properties: the Inangahua, New Zealand aftershocks of 1968. *Bull. Seism. Soc. Am.,* vol. 65. 1975. pp. 261–276.
15. BRUMMER, R.K., and RORKE, A.J. Case studies on large rockbursts in South African gold mines. *Rockbursts and seismicity in mines.* Fairhurst (ed.). Rotterdam, Balkema, 1990. pp. 323–329.
16. HANKS, T.C., and KANAMORI, H. A moment amplitude scale. *J. Geophys. Res.,* vol. 84. 1979. pp. 2348–2350.
17. SPOTTISWOODE, S.M. Personal communication.

The three-dimensional model was used to investigate the variance of the hangingwall velocity amplification factor over a 60 x 60 m stope. The carpet plot in Figure 13 shows the absolute amplification (the square root of the sum of the squared horizontal and vertical amplification factors) of the hangingwall velocity over the stope plane.

Most of the hangingwall is subjected to an absolute amplification factor of approximately 3. However, the velocities in the corners of the stope-back area are amplified 5 times. Hemp and Goldbach[19] measured amplification factors in deep mines of up to 5,3 and 9,9. The numerical modelling showed that localized stope areas can be subjected to much higher amplification factors than the rest of the stope.

The amplification factors calculated by the elastic WAVE analyses are due to the Rayleigh waves propagating along stope surfaces. Further modelling is necessary so that the elastic analyses can be extended to numerical models that incorporate footwall and hangingwall fractures, from which the effect of stope fractures on amplification factors can be evaluated.

Although localized stope areas might experience high velocity amplification, the highest velocities need not necessarily occur there. This is shown by plots of the absolute hangingwall velocity over the stoping extent. Figure 14 gives a carpet plot of the absolute velocity in centimetres per second.

By the time the shear wave containing the peak velocities has propagated to the stope-back area, the velocities have attenuated to such an extent that, although amplified by a factor of 5, the absolute velocities are small compared with velocities in the rest of the stope. For the stope–fault geometry investigated in this study, the maximum velocities occur in an area 10 to 20 m from the stope face.

By means of numerical modelling, amplification factors and peak velocities of typical mining layouts can be calculated, and potentially hazardous stope regions subjected to high velocities can be identified. Such regions require additional local support and close monitoring of the rock conditions. Thus, numerical modelling has the potential to provide essential information in the classification of hazardous areas and the initiation of special precautions.

Conclusions

From the findings of this study, the following conclusions are drawn.

(1) WAVE is an efficient numerical tool for the modelling of fault slip and wave propagation.

(2) The far-field peak velocity comparisons showed that
   - the two-dimensional plane-strain assumption over-estimates the peak velocities compared with the analytical solution of Brune[1,2] and McGarr's empirical relationship[3]

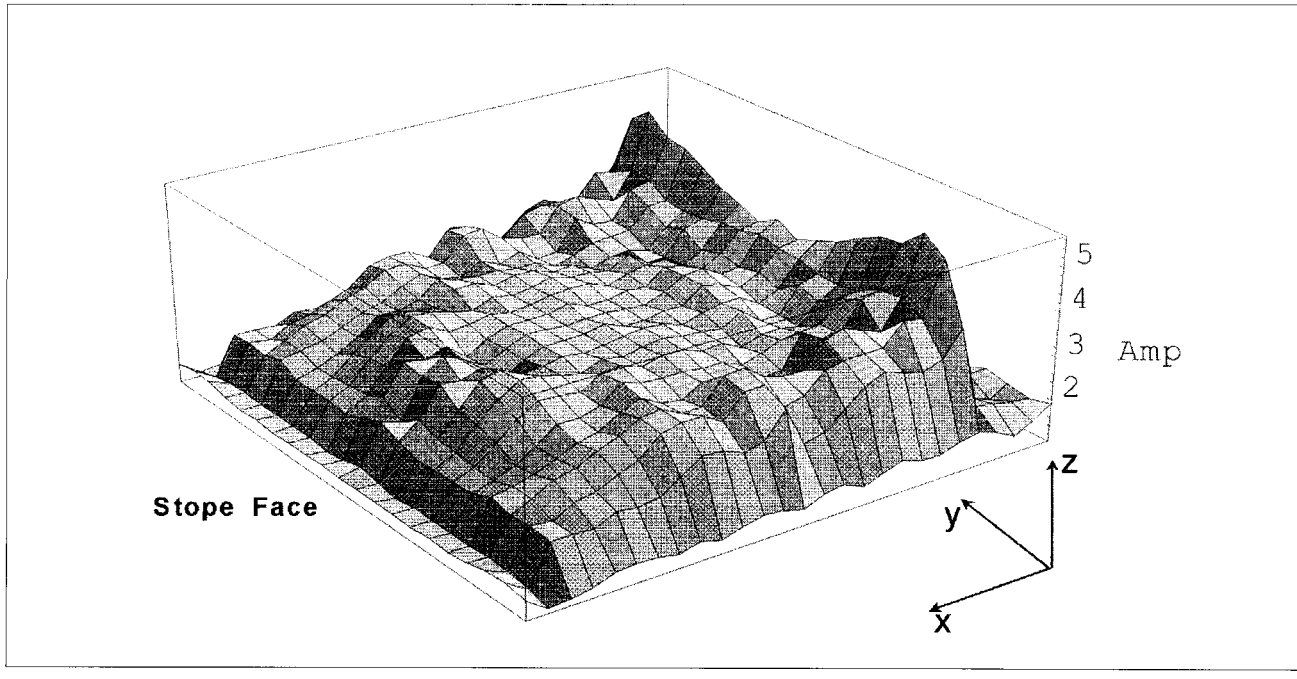

Figure 13—Absolute hangingwall velocity amplification factor over the stope plane

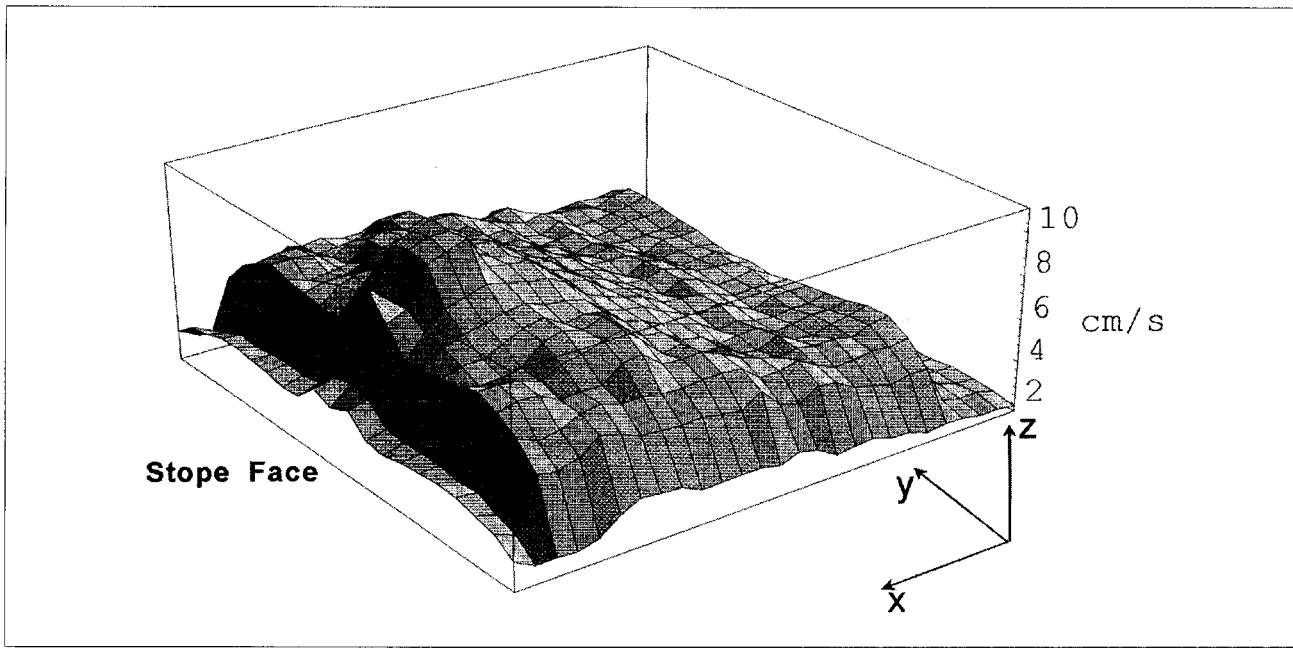

Figure 14—Absolute hangingwall velocity

18. SJÖBERG, J. Numerical analysis of a fractured rock mass response to the dynamic loading by fault slip. *Rock engineering consultancy report.* Johannesburg, Chamber of Mines Research Organization, 1993.
19. HEMP, D.A., and GOLDBACH, O.D. The effect of backfill on ground motion in a stope. *Rockbursts and seismicity in mines.* Young (ed.). Rotterdam, Balkema, 1993. pp. 75–79.

- velocities calculated by the three-dimensional WAVE model with instantaneous fault rupture compare well with the analytical solution of Brune[1,2]
- when the appropriate slip-weakening rate is chosen, peak particle velocities of the three-dimensional WAVE analyses correlate closely with seismological field data.

(3) In the near-field, this study concludes that

- velocity amplification factors calculated by WAVE compare well with the actual values measured by Spottiswoode and Churcher[4]
- numerical modelling is an essential tool for the identification of potentially hazardous stope areas prone to excessive velocities; for the three-dimensional stope–fault geometry investigated in this study, the maximum velocities occurred in an area 10 to 20 m from the stope face.

As a result of the findings and conclusions, the following recommendations are made.

(a) Actual mining layouts need to be modelled in three dimensions so that stope areas prone to high seismic velocities or peak ground velocities are identified.
(b) A parametric study should be conducted to evaluate the influence of a softened zone around the stope and to simulate the effects of horizontal parting planes and vertical shear fractures on amplification factors and peak velocities. ◆